Rupture Characteristics of the Deep Bolivian Earthquake of 9 June 1994 and the Mechanism of Deep-Focus Earthquakes

Paul G. Silver, Susan L. Beck, Terry C. Wallace, Charles Meade, Stephen C. Myers, David E. James, Randy Kuehnel

The M_w = 8.3 deep (636 kilometers) Bolivian earthquake of 9 June 1994 was the largest deep-focus earthquake ever recorded. Seismic data from permanent stations plus portable instruments in South America show that rupture occurred on a horizontal plane and extended at least 30 by 50 kilometers. Rupture proceeded at 1 to 3 kilometers per second along the down-dip azimuth of the slab and penetrated through more than a third of the slab thickness. This extent is more than three times that expected for a metastable wedge of olivine at the core of the slab, and thus appears to be incompatible with an origin by transformational faulting. These large events may instead represent slip on preserved zones of weakness established in oceanic lithosphere at the Earth's surface.

Deep-focus earthquakes occur exclusively in subducted oceanic lithosphere. Slip appears to take place on fault planes, and rupture propagates at 1 to 4 km/s, as with surface events. Frictional sliding, the mechanism that causes earthquakes at shallow depths, is restricted to pressures lower than about 1 to 2 GPa (depths of 30 to 60 km); at high pressures and temperatures, faulting is expected to be replaced by ductile deformation (*1*). These deeper events then require a separate mechanism that nevertheless produces earthquakes much like their shallow counterparts. Efforts have focused two candidate mechanisms: the metastable transformation of olivine to the denser spinel structure (*2–4*) and dehydration of hydrous minerals (*5*, *6*). Details of the phase transformation hypotheses have advanced to the stage where a test can be formulated. In this report we provide such a test, based on the rupture properties of the very largest deep-focus events.

On 9 June 1994, the largest (M_w = 8.3) recorded deep-focus earthquake occurred beneath Bolivia at a depth of 636 km (NEIC). It was recorded by the recently deployed global network of digital broadband high-dynamic-range seismographs and three networks of portable broadband instruments in South America [Fig. 1A (*7*)]. The stations from the BANJO/SEDA (Broadband ANdean JOint/Seismic Examination of the Deep Altiplano) experiments (*8*) were just a few hundred kilometers south of this earthquake, and the BLSP (Brazilian Lithospheric Seismic Program) stations (*9*) were some 1500 km to the ESE in Brazil (Fig. 1B). Because most permanent seismic stations are in the Northern Hemisphere, there is usually poor coverage at southern azimuths for these large South American events. Thus, the addition of the portable instrumentation adds critical coverage in the southeast quadrant, and provided an opportunity to study this event in detail (Fig. 1C).

The rupture properties of a seismic event can be inferred through analysis of directivity, the station-to-station variation in the observed signal from an earthquake due to the finite size of the faulting region (*10–12*). Where rupture proceeds in one direction (unilateral rupture), the displacement pulse observed at any station i will vary in duration T (although with identical pulse shape) according to

$$T^i = \tau - (X/c)\cos\Delta^i \qquad (1)$$

(*13*), where Δ^i is the angular distance between the rupture velocity vector $\mathbf{V}$ and the propagation direction $\hat{\mathbf{p}}^i$ at the source, c is the propagation velocity (either P or S wave), τ is the actual duration of moment release, and X is the total rupture extent. If the rupture is not strictly unilateral, then we can instead identify individual subevents with times $T_1^i, T_2^i \ldots$ which can be individually inverted as in Eq. 1 (*10*). T_n^i is then interpreted as the arrival time of the subevent, τ_n is its origin time, X_n is the distance from the location of the onset of rupture to the subevent, and Δ_n^i is the angle between $\hat{\mathbf{p}}^i$ and the relative location unit vector $\hat{\mathbf{x}}_n$ of the subevent with respect to the onset. We performed this second analysis of P-wave (Fig. 2) and some S-wave displacement traces for the Bolivian event. With measurements of T_i and given that $\hat{\mathbf{p}}^i$ and c are known from the source-receiver geometry and a velocity model for the Earth, Eq. 1 can be used to estimate the remaining four variables, τ, X, and the two

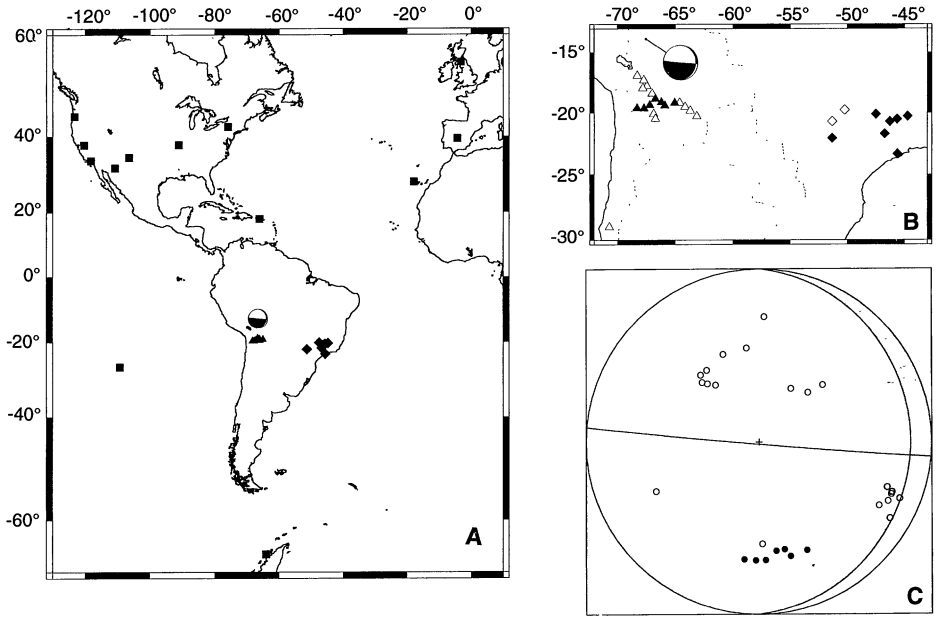

Fig. 1. (**A**) Locations of the stations used in constraining the rupture properties of the Bolivian earthquake. Triangles and diamonds denote BANJO/SEDA and BLSP portable stations. Squares give the locations of permanent stations. Also shown, location and source mechanism (*15*) of Bolivian event. (**B**) All portable stations that recorded the event. Filled symbols are those stations actually used (based on being on-scale and within appropriate distance range). (**C**) Focal sphere plot of the stations used. Open circles are for down-going rays (lower hemisphere projection, permanent stations, and BLSP), filled circles are for up-going rays (upper hemisphere projection, BANJO stations).

P. G. Silver, D. E. James, R. Kuehnel, Carnegie Institution of Washington, Department of Terrestrial Magnetism, 5241 Broad Branch Road, Northwest, Washington, DC 20015, USA.
S. L. Beck, T. C. Wallace, S. C. Myers, Southern Arizona Seismic Observatory, Department of Geosciences, University of Arizona, Tucson, AZ 85721, USA.
C. Meade, Carnegie Institution of Washington, Geophysical Laboratory, 5251 Broad Branch Road, Northwest, Washington, DC 20015, USA.

angles θ (measured from the horizontal, positive up) and ϕ (clockwise from north) defining $\hat{\mathbf{x}}_n$.

The Bolivian event began with a small onset in moment release for 10 s followed by a large pulse lasting ~40 s. Within the large pulse we observed at least four subevents (Fig. 2). The station-to-station differences in arrival times of these subevents allow us to characterize the rupture characteristics. For example, the large pulse (labeled T1 in Fig. 2) arrived earlier at stations in Brazil (ESE), compared to stations at other azimuths, constituting clear evidence of directivity toward the east.

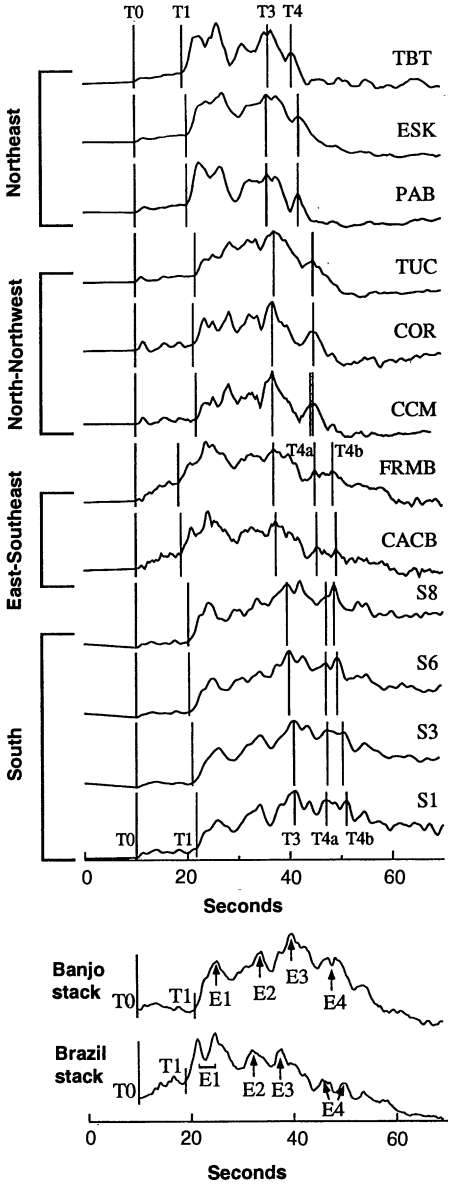

Fig. 2. (**Top**) Representative displacement records used in inversion. Note coherence of waveforms within each group of stations and the clear differences between groups. The difference in waveforms suggests that it is not a simple unilateral rupture. Shown in all cases are the estimated arrival times T_0, T_1, T_3, T_{4a}, and T_{4b} (see text). (**Bottom**) Stacks of displacement records from the BANJO and BLSP stations. On the stacks are noted the various subevents that comprise the source pulse.

We chose five reference times in the displacement P waveforms that correspond to critical points in the rupture process. These are (Fig. 2 and Table 1): T_0, the onset time of the event (E_0), which we use as a reference for all subsequent subevents, T_1, the initiation time of the first subevent (E_1) some 11 s into the record, T_3, the time of peak moment release (E_3), and T_4 the last significant moment release (E_4) about 35 to 40 s from the onset. This last pulse clearly bifurcates into two distinct peaks for most of the stations: all stations to the south (all BANJO and BLSP records plus PMSA and RPN) and those to the north-northwest (SJG, CCM, and ANMO). This bifurcation is not seen to the northeast (TBT, PAB, and ESK) and is ambiguous for stations to the northwest. We thus refer to these as distinct subevents E_{4a} and E_{4b} (with times T_{4a} and T_{4b}) and assume that they arrive at the same time for stations where two subevents could not be resolved.

Using Eq. 1 we located these subevents with respect to the onset of rupture by performing a linear inversion for τ and X and a grid search over all possible values of θ and ϕ in 5° increments. We minimized the squared misfit between predicted and observed delay times, and used the misfit contours to determine uncertainties (*14*). As a first step in estimating rupture geometry, we performed an unconstrained inversion for subevent location to determine if either the near-horizontal (P_h) or near-vertical (P_v) nodal plane [strike, dip, rake = (1°, 13°, −4°) and (95°, 89°, −103°), respectively (Fig. 1) (*15*)], was also the rupture plane. The best fit θ values for all four events are near-horizontal: θ = (−10°, −10°, −5°, 10°) for E_1, E_3, E_{4a}, and E_{4b}, respectively. As shown by the estimates of (θ, ϕ) (Fig. 3A), all four subevents are consistent with P_h (Fig. 3A), and all but E_1 are inconsistent with P_v (E_1 can be fit by either plane). We thus conclude that rupture occurred on P_h. To further resolve the rupture properties, we reinverted for the subevent location, constraining the subevents to lie on P_h. (Table 2; results are similar if a horizontal plane is used instead). Uncertainty in X is illustrated by plotting the directivity parameter defined as $\Gamma^i = (\cos\Delta^i)/c$ against reduced delay time $T^i - \tau$ (Fig. 3A). As in Eq. 1, this should be a straight line for the optimal solution, with a slope of X. E_1 and E_3 show little scatter, although E_{4a} and E_{4b} show increased scat-

Table 1. Seismic stations and data. Sta., stations; Lat., latitude; and long., longitude. Latitude and longitude are in degrees.

Sta.	Lat., long.	T_1 (s)	T_3 (s)	T_{4a} (s)	T_{4b} (s)
		South			
S01	−19.61, −68.33	11.72	30.97	36.98	41.00
S02	−19.62, −67.73	11.58	30.4	37.34	41.00
S03	−19.35, −67.22	11.30	30.8	37.31	40.65
S04	−18.83, −66.73	11.10	30.2	36.75	39.76
S05	−19.10, −66.22	10.80	29.9	37.00	39.96
S06	−19.38, −65.93	10.86	29.9	37.04	39.26
S08	−19.16, −65.07	10.20	29.5	38.66	38.66
PMSA	−64.77, −64.05	10.7	30.0	35.7	41.1
		East-southeast			
CACB	−21.68, −46.73	8.8	27.4	35.37	39.11
CDCB	−20.24, −44.72	—	—	35.37	38.95
FRMB	−20.49, −45.64	8.3	27.03	35.02	38.59
FURB	−20.68, −46.28	8.7	27.33	35.12	38.92
PARB	−23.34, −45.62	8.5	27.7	35.40	39.24
PPDB	−22.03, −51.31	8.8	—	—	—
RIFB	−20.07, −47.50	8.4	26.91	34.52	38.52
		North-northwest			
ANMO	34.95, −106.46	11.9	27.10	32.85	34.70
BINY	42.20, −75.99	11.4	—	—	—
CCM	38.06, −91.25	11.8	26.9	34.20	34.70
CMB	38.04, −120.39	11.8	27.65	35.28	35.28
COR	44.59, −123.30	11.7	26.85	34.85	34.85
PAS	34.15, −118.17	11.5	27.50	34.30	36.10
SJG	18.11, −66.15	10.4	25.8	32.85	34.16
TUC	32.31, −110.78	11.9	27.60	34.74	34.74
		Northeast			
ESK	55.32, −3.21	10.0	25.7	32.00	32.00
PAB	39.55, −4.35	10.1	25.75	32.88	32.88
TBT	28.68, −17.91	9.3	26.10	30.65	30.65
		Southwest			
RPN	−27.23, −109.33	12.8	29.0	38.2	39.7

ter, reflecting the lower signal levels for these subevents.

All subevents occurred in the northeast quadrant (Fig. 3C); E_1 was the most easterly, 29 km east of E_0 (apparent rupture velocity, 2.6 km/s). The subsequent events occurred roughly north of E_1; E_{4b} had the greatest extent (X = 52 km). The apparent rupture velocity for these later events were all much lower, from 1.0 to 1.4 km/s. Thus, the rupture extent was about 30 by 50 km with the long direction oriented to the north-northeast. A partial check of this geometry is available from the S-wave data. Because the S waves were generally noisier, it was only possible to reliably pick times for T_1 and T_3. The location of E_3 with respect to E_1 was $\phi = -20°$ and X = 32 km, which when combined with the location of E_1 from the P waves gives $\phi = 31°$ and X = 35 km with respect to E_0. These values are close ($\phi = 35°$, X = 34 km) to the parameters obtained for E_3 directly from P waves (Table 2). The inferred geometry is also similar to that obtained from teleseismic data by Kikuchi and Kanamori (*15*). They also concluded that the near-horizontal plane provided the best fit to the data and that the rupture propagated to the northeast. Our rupture dimensions are somewhat larger than those of (*15*), because of the enhanced coverage to the south and east provided by the local stations (*16*).

Table 2. Inversion for rupture properties. Four subevents identified in waveforms for which rupture properties were determined (see text). X and ϕ are the distance and azimuth (clockwise from north) referenced to onset E_0. τ is origin time of subevent and V is apparent rupture velocity X/τ. Rupture plane assumed to be near-horizontal nodal plane (*15*). Uncertainties are 1σ. N is number of observations.

Event	X (km)	ϕ (deg)	τ (s)	V (km s^{-1})	N
E_1	29 ± 3	90 ± 5	11.1	2.6 ± 0.2	26
E_3	34 ± 3	35 ± 5	28.0	1.2 ± 0.2	25
E_{4a}	35 ± 7	30 ± 13	35.1	1.0 ± 0.2	25
E_{4b}	52 ± 9	15 ± 10	36.8	1.4 ± 0.3	25

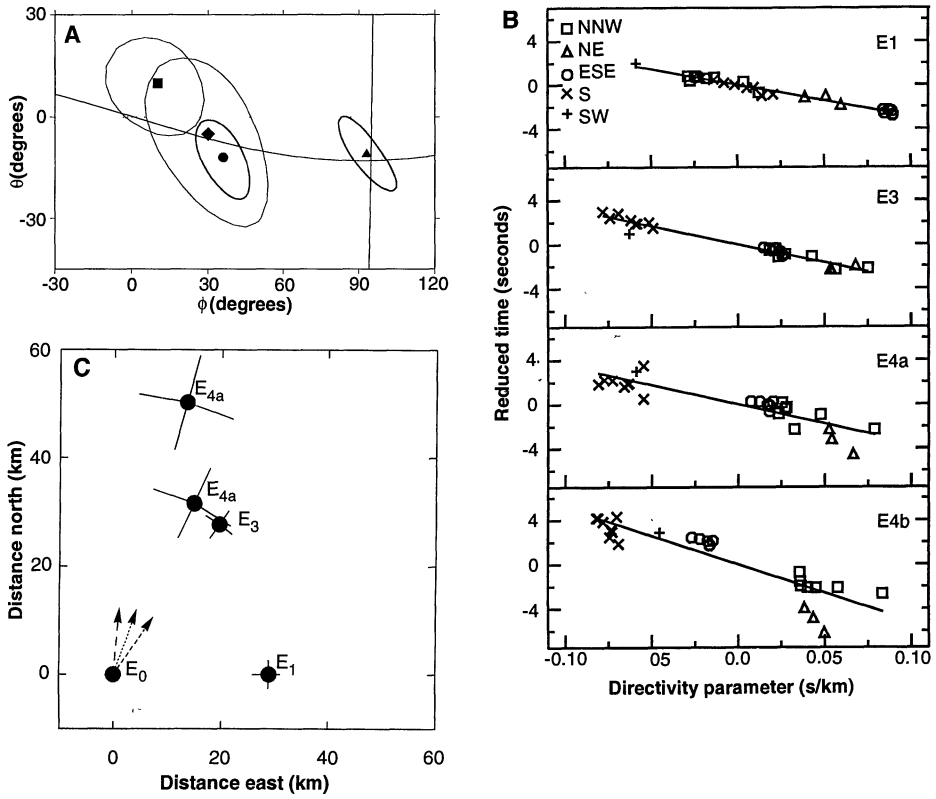

Fig. 3. Inversion for rupture properties (see Table 2). (**A**) Estimates and 95% confidence contours (marginal uncertainties) for inclination angle θ (measured positive up from horizontal) and azimuth ϕ (measured clockwise from north); for unconstrained inversion for subevents E_1 (triangle), E_3 (circle), E_{4a} (diamond), and E_{4b} (square). Darker contours are for better constrained subevents E_1 and E_3, and lighter contours are for less well-constrained subevents E_{4a} and E_{4b}. Near-horizontal (P_h) near-vertical (P_v) solid curves correspond to estimated nodal planes for this event (*15*). Dotted line is horizontal plane. All events are consistent with occurrence on (P_h), and, except for E_1, are inconsistent with occurrence on (P_v). (**B**) Plot of directivity parameter Γ versus reduced delay time ($T^{-1} - \tau$) for the four subevents corresponding to the solutions in Table 2 (see text). The slope of the line equals the distance X and scatter reflects the related uncertainty. Symbols identify station azimuth (legend). (**C**) Map view of subevent locations with respect to the onset, along with 1σ uncertainties. Also shown, azimuth of compression axis of source mechanism [long dash (*15*)], inferred down-dip azimuth of slab from recent deep focus seismicity (dotted) and aftershock seismicity (short dash (*17*). Long direction of rupture is roughly parallel to these directions.

The deep-focus seismicity of South America is concentrated in two nearly north-south lines. The northern part of the southern line is offset some 500 km to the east, separated by a comparatively aseismic region between 11° and 16° south (Fig. 4). The Bolivian event occurred in this region. The deep geometry of the slab here is revealed by the recent increased seismicity associated with the event, two other events in 1994 (10 January and 8 August), and numerous aftershocks (*17*). Further information is available from conversions and reflections from the top surface of the slab using data from local portable stations (*18*). We modified contours of derived slab consistent with these data. At 600 km, the slab appears to be dipping ~45° toward N20°E. This geometry is supported by two additional observations. First, the aftershock distribution (*17*) is not confined to the horizontal rupture plane, but also appears to represent increased seismicity in the slab from ~15 km above to ~25 km below the event. The aftershocks define a plane dipping 45° toward N35°E, roughly parallel to the inferred slab. Second, for this geometry the maximum compressive stress direction as inferred from the source mechanism of the Bolivian earthquake is down-dip, the orientation most often found for deep focus events (*19*).

The horizontal extent of the Bolivian earthquake is at least 50 km along the down-dip azimuth (*20*). Rupture proceeded from the center of the slab toward its former top surface, cutting the slab at a 45° angle. The rupture thus penetrated about 35 km of the slab's thickness. Deep focus events of this size are rare; the last one occurred some 25 years ago, roughly 1000 km to the north of this event beneath Colombia (*10, 11, 21*). Similarities with the Bolivian event are striking. The Colombian event ruptured the westward-dipping nodal plane (dip angle of 45°). The subevents were distributed primarily up-dip from the main event extending ~60 km (in an east-west cross section) with an overall duration of about 50 s (rupture velocities of 1.0 to 3.2 km/s (*10*)). The slab geometry is less well constrained than for Bolivia because of the absence of nearby seismicity. The near-vertical compression axis for this event (*21*), a steeply dipping slab (*22*), and the

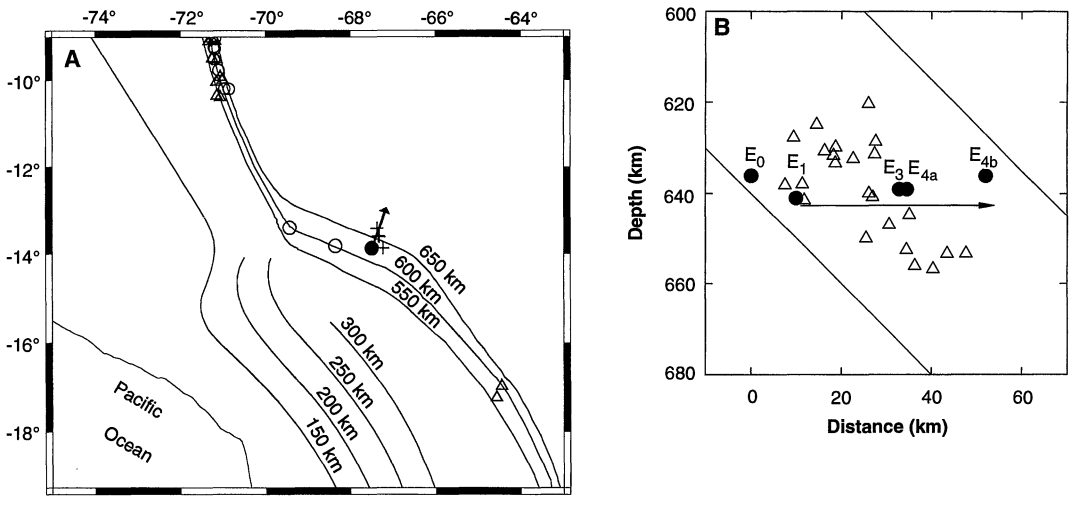

Fig. 4. (**A**) Relocated deep focus seismicity (*40*) in the depth range 500 to 600 km (triangles) and greater than 600 km (circles), along with slab contours. Shallow contours from (*41*) (150 km to 300 km) and deeper ones are from (*18*), modified to be consistent with recent Bolivian seismicity in 1994 (10 January and 8 August, two open circles in middle of plot). Also shown, the NEIC location of the main event (filled circle), the estimated locations of four subevents (crosses), and inferred down-dip azimuth of slab, N20°E (arrow). (**B**) Cross section taken parallel to arrow in (A), showing estimated locations of subevents (filled circles) along with distribution of aftershocks (*17*). Diagonal lines give approximate dip of slab (45°) and bound region of slab containing subevents and aftershocks. In cross section, rupture extent is about 50 km. Apparent rupture direction is toward the former top surface of the slab (direction of arrow). Rupture penetrated 35 km of slab thickness.

north-south trend of deep-focus seismicity a few hundred kilometers to the south all suggest that the slab here is striking roughly north-south and dipping steeply to the east. The rupture also evidently proceeded from the core of the slab toward its former top surface. The inferred slab thickness penetrated by the event is at least 45 km, comparable to (indeed larger than) the Bolivian event. A somewhat smaller (M_w = 7.6) deep-focus event occurred recently beneath Tonga that also ruptured a comparable thickness of the slab (*23*).

According to the transformational faulting hypothesis for deep-focus earthquakes (*2, 3, 24, 25*), olivine in the slab is metastably subducted below the equilibrium depth of the olivine → γ-spinel phase transition (400 km). Deep seismicity is driven by a shear instability associated with the olivine-spinel phase transformation in a metastable wedge (Fig. 5). The termination of earthquakes near 650 km is thought to represent the complete transformation of metastable olivine to spinel in the subducting slab (*26*). Outside of the wedge, a rupture on a fault would be presumably stopped by friction.

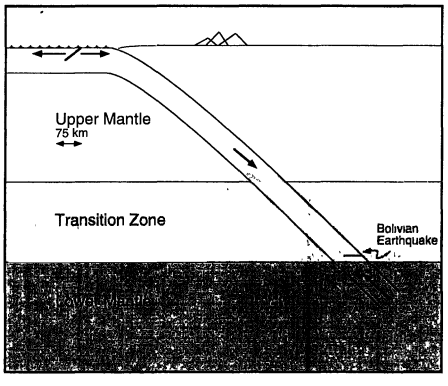

Fig. 5. Schematic of transformational faulting hypothesis. As slab descends, the mineral olivine (white) transforms to denser spinel phase (gray) in transition zone. It is hypothesized that there exists a metastable wedge of olivine, within which deep focus earthquakes occur. Shown is approximate shape of wedge appropriate for South American slab. The rupture extent of Bolivian earthquake (shown in text) is much larger than the thickness of the metastable region. Alternatively, large deep-focus earthquakes could occur on preserved zones of weakness that have originally formed during large normal-faulting earthquakes in the oceanic lithosphere seaward of subduction zones (shown at top).

The size of this metastable wedge will be governed by the kinetics of the olivine-spinel phase transformation and the thermal structure of the slab. For compositions of $(Mg_{0.9}, Fe_{0.1})_2SiO_4$ at 13.3 GPa (corresponding to 400-km depth in the mantle) the temperature for the transition α-olivine → α-olivine + γ-spinel is 1000° to 1400°C. The uncertainty in the transition temperature reflects the size of the mixed phase region in the MgO − FeO − SiO_2 system and kinetics. A broad range of kinetic experiments on the olivine-spinel transition indicate that the maximum temperature for preserving metastable olivine at the base of the upper mantle (P = 15 to 23 GPa) is approximately 600°C (*27, 28*). For the transformational faulting hypothesis to be valid, the seismically active portions of subducting slabs must remain below this temperature before faulting.

Thermal models of subduction zones show that thermal evolution is most strongly dependent on the age of the slab and the subduction velocity. For the South American slab, or even much colder slabs (*29*), the width of the 600°C isotherm, and hence the thickness of the proposed metastable wedge of olivine, is predicted to be ≤10 km and may not even be present at the depth of the Bolivian earthquake. This is considerably less than the thickness of slab ruptured by the earthquake, 35 km.

Several seismological studies have searched for the predicted properties of the metastable olivine wedge: low seismic velocities in the core of the wedge (*30*) and concentrated seismicity at its boundary (*31*). Even if such a wedge exists, however, it does not prove that transformational faulting is occurring. The most important requirement is that all deep-focus events should be contained within the wedge. The Bolivian event ruptured well outside the likely metastable zone, regardless of where the rupture occurred in the slab. The properties of the Colombian event and recent Tonga event lead to the same conclusion. These results taken together rule out any mechanism that relies solely on a metastable phase transformation in olivine.

To reconcile the rupture characteristics of the Bolivian earthquake with the transformational faulting hypothesis would require either (i) that the slab is horizontal at the base of the upper mantle or (ii) that the metastable wedge is anomalously thick (>35 km). As discussed above, (i) is inconsistent with the geometry of the slab at the depth of the earthquake, as well as the sense of slip during the Bolivian event, and regional tomographic studies (*32*). Even if the slab were flat, the depth range of aftershocks would still imply a seismic zone 30 to 40 km in thickness. (ii) can be achieved either by a thickened slab or a metastable wedge comprising a larger portion of an underformed slab. Although slab thickening has been inferred for the lower mantle based on seismic tomography (*22*) and geoid modeling (*33*), there is no evidence for thickening in the upper mantle. Laboratory and numerical experiments (*34*) indicate that any thickening

would occur by folding, which would not affect the thickness of the metastable wedge (*35*). A thickened metastable wedge in an undeformed slab would present serious dynamical problems. In particular, with a 35-km-thick wedge of olivine, a 100-km-thick slab would be positively buoyant between 400 and 650 km depth and should not sink at all (*36*).

The size and orientation of the rupture plane of the Bolivian earthquake are broadly similar to those of the largest earthquakes that occur in the oceanic lithosphere at the Earth's surface. Bending or lithospheric normal-faulting events that occur near the trench wall or on the outer rise just before subduction, can have magnitudes in excess of $M_w = 8$ (*37*). In the case of the Sumbawa earthquake of 1977 ($M_w = 8.3$), for example, the normal faulting produced a rupture plane dipping 45° and extending from the surface to depths of 30 to 50 km (*38*). Both events occurred on the surface of maximum shear stress for in-plane stresses in the lithosphere, and in both cases the largest principal stress direction (tensional for Sumbawa, compressional for Bolivia) was parallel to the down-dip direction of the slab. The similarity of these deep and shallow events suggests that failure during deep-focus earthquakes represents the reactivation of faults that were established when the lithosphere was near the Earth's surface (*39*). Several processes might preserve the weakness of established faults zones to depths of 650 km, such as a reduction in grain size by the faulting process or dehydration of hydrous minerals initially produced by the circulation of fluids into the fault zone (*6*). The hypothesis that deep events occur on preexisting faults addresses perhaps the most intriguing and paradoxical feature of deep focus events, namely their striking resemblance to earthquakes near the Earth's surface.

REFERENCES AND NOTES

1. C. Scholz, *The Mechanics of Earthquakes and Faulting* (Cambridge Univ. Press, Cambridge, 1990).
2. S. Kirby, *J. Geophys. Res.* **92**, 13,789 (1987).
3. H. W. Green and P. C. Burnley, *Nature* **341**, 733 (1989).
4. H. W. Green *et al.*, *ibid.* **348**, 720 (1990); H. W. Green *et al.*, *Geophys. Res. Lett.* **19**, 789 (1992); C.-M. Sung and R. G. Burns, *Tectonophysics* **31**, 1 (1976); *High Pressure Science and Technology* (Plenum, New York, 1979): To depths of 700 km in the mantle $(Mg,Fe)_2SiO_4$ olivine transforms to β-$(Mg,Fe)_2SiO_4$, γ-spinel, and an assemblage of $(Mg,Fe)SiO_3$ perovskite and (Mg,Fe)O [R. Jeanloz and A. Thompson, *Rev. Geophys. Space Phys.* **21**, 51 (1983)]. Because the minimum depth for these transitions is 400 km, phase transitions in olivine are only applicable to earthquakes in the transition zone.
5. C. B. Raleigh and M. S. Paterson, *J. Geophys. Res.* **70**, 3965 (1965); C. B. Raleigh, *Geophys., J. R. Astron. Soc.* **14**, 113 (1967).
6. C. Meade and R. Jeanloz, *Science* **252**, 68 (1991).
7. The last comparably sized deep event, the Columbia earthquake of 1970 (*10, 11, 21*), was recorded by analog instruments possessing a more limited dynamic and frequency range. The three networks of portable broadband instruments in South America obtained high-quality on-scale recordings of the Bolivian event. Data from passive experiments now rival in quality the data obtained from permanent observatories.
8. S. L. Beck *et al.*, *IRIS Newsl.* **8**, 1 (1994).
9. D. E. James and M. Assumpção, *Eos* **74**, 202 (1993).
10. M. Furumoto, *Phys. Earth Planet. Inter.* **15**, 1 (1977).
11. R. A. Strelitz, *ibid.* **21**, 83 (1980).
12. A. Ben-Menahem, *Bull. Seismol. Soc. Am.* **51**, 401 (1961). *J. Geophys. Res.* **67**, 345 (1962); F. Press, A. Ben-Menahem, M. N. Toksoz, *ibid.* **66**, 3471 (1961); N. A. Haskell, *Bull. Seismol. Soc. Am.* **54**, 1811 (1964); P. G. Silver, *ibid.* **73**, 1499 (1983); P. G. Silver and T. Masuda, *J. Geophys. Res.* **90**, 7639 (1985); S. L. Beck and D. H. Christensen, *ibid.* **96**, 2205 (1991); M. Kikuchi and H. Kanamori, *Bull. Seismol. Soc. Am.* **72**, 491 (1982); *ibid.* **81**, 2335 (1991).
13. K. Aki and P. Richards, *Quantitative Seismology: Theory and Methods* (Freeman, San Francisco, CA, 1980).
14. Uncertainties in the parameters are found by determining the critical level of squared misfit S at the 95% confidence level using the formula $S/S_{min} \leq 1 + (k/(n-k))f_{k,n-k}(1-\alpha)$ [G. M. Jenkins, and D. G. Watts, *Spectral Analysis and Its Applications* (Holden-Day, San Francisco, CA, 1968)] where S_{min} is the minimum value of S, n is the number of data points, k is the number of parameters, and f is the inverse of the F distribution. In our specific case $\alpha = 0.05$ and k is set to 3 if the rupture is constrained to lie on a plane or 4 if not constrained.
15. M. Kikuchi and H. Kanamori, *Geophys. Res. Lett.* **21**, 2341 (1994).
16. E_1, the initiation of major moment release, is 29 km from the onset in our data [compared to only 20 km (*15*)]. This is primarily constrained by the extremely early values for T_1 from BLSP stations (Fig. 2) that were in the direction of rupture for this subevent. Subsequent events are some 10 to 20 km more northerly than found in (*15*), because of the constraints from the BANJO stations to the south.
17. S. C. Myers *et al.*, *Geophys. Res. Lett.*, in press.
18. I. S. Sacks, *J. Geophys. Res.* **88**, 3355 (1983).
19. B. Isacks and P. Molnar, *Rev. Geophys. Space Phys.* **9**, 103 (1971).
20. A different analysis that is primarily applicable to directivity within one subevent, suggests that E_1 ruptured about 10 km to the south from its onset position in Fig. 3C. This would make the overall rupture dimension closer to 60 km (S. Beck *et al.*, *Geophys. Res. Lett.*, in press).
21. J. A. Mendiguren, *Geophys. J. R. Astron. Soc.* **33**, 281 (1973); F. Gilbert and A. M. Dziewonski, *Philos. Trans. R. Soc. London Ser. A* **278**, 187 (1975).
22. S. Grand, *J. Geophys. Res.* **99**, 11,591 (1994).
23. D. Weins *et al.*, *Nature* **372**, 540 (1994).
24. S. H. Kirby *et al.*, *Science* **252**, 216 (1991).
25. H. W. Green, *Sci. Am.* **271**, 3 and 64 (September 1994); C. Frohlich, *Nature* **368**, 100 (1994).
26. On the basis of laboratory experiments (*3*), it has been postulated that small lens-shaped zones of spinel form in the metastable olivine wedge. Because of the self-sustaining stresses associated with their growth, these lenses are termed anticracks. They are presumed to be mechanically weak so that they promote shear failure under an applied stress.
27. D. Rubie *et al.*, *Phys. Earth Planet. Int.* **86**, 223 (1994); A. E. Ringwood, *Geochim. Cosmochim. Acta* **13**, 303 (1958); K. Suito, *High Pressure Research, Application in Geophysics* (Academic Press, New York, 1979); M. D. Furnish and W. A. Bassett, *J. Geophys. Res.* **88**, 10,333 (1983); D. C. Rubie *et al.*, *ibid.* **95**, 15,829 (1990).
28. T. C. Wu *et al.*, *J. Geophys. Res.* **98**, 19,767 (1993).
29. The thermal structure of the slab primarily depends on the age of lithosphere being subducted and the vertical descent rate. The Japan slab is much colder than the South American slab, and thus should provide an upper bound on the width of the metastable zone. Maximum depths of the 600°C and 700°C isotherms are about 550 and 650 km (*24*). Thus the metastable wedge should be thin or nonexistent at the depth of the Bolivian earthquake. Even the Tonga slab, which is the coldest of any slab [S. Stein *et al.*, *SUBCON Conference* **307** (1994)] has a 600°C isotherm that is only about 10 km thick at a depth of 636 km (S. Stein, personal communication).
30. T. Iidaka and D. Suetsugu, *Nature* **356**, 593 (1992). These authors reported the presence of a low-velocity channel in the slab beneath Japan, which was interpreted as being the metastable wedge.
31. D. A. Weins, J. J. McGuire, P. J. Shore, *ibid.* **364**, 790 (1993). These authors have observed a double seismic zone in the Tonga slab at 350 to 460 km, which may mark the wedge boundary. The existence of a double seismic zone, however, is not necessarily evidence for a metastable wedge. Such zones have also been detected at shallower depths. In (*30*), the low-velocity channel could reflect other variations in structure near the slab.
32. The sense of slip on the horizontal plane for the Bolivian event implies that the bottom of the fault zone is moving south with respect to the top. This is consistent with the steepening of the slab, rather than flattening at this depth. Seismic tomography (*22*) suggests that, at least just north of this event, the slab descends into the lower mantle and shows no indication of turning horizontally. A more recent tomographic study of the area of the Bolivian event itself is consistent with the slab penetrating into the lower mantle and not turning horizontally. E. R. Engdahl *et al.*, *Geophys. Res. Lett.*, in press.
33. Y. Ricard *et al.*, *Geophys. Res.* **98**, 21,895 (1993).
34. L. Guilloi-Frottier, J. Buttles, P. Olson, *Earth Planet. Sci. Lett.*, in press; R. W. Griffiths and J. S. Turner, *J. Geophys. Res.* **93**, 397 (1988).
35. If indeed shortening of this factor could take place in a homogeneous manner, in the coldest core of the slab, then the shear heating associated with this deformation would be significant, as both strains and deviatoric stresses would be high (C. Kincaid and P. G. Silver, in preparation). Strains of order unity (doubling) at a stress of 100 MPa would produce a 30° increase in temperature. But deviatoric stresses of as high as 2 GPa have been proposed for the core of the slab [K. Goto, Z. Suzuki, H. Hamaguchi, *J. Geophys. Res.* **92**, 13,811 (1987)] in conjunction with the metastable wedge, suggesting a rise in temperature of several hundred degrees. This heating would effectively remove the metastable wedge. Finally, deviatoric stress tends to lower the temperature at which the transition occurs (*28*). This again serves to reduce the size of the metastable zone.
36. The density difference between olivine and spinel is about 6% (*24*). Assuming that the coefficient of thermal expansion is 3×10^{-5} °C^{-1}, that the slab is on average 500° cooler than the ambient mantle, and that the metastable region constitutes a third of the slab, then the combined slab would be positively buoyant by about 0.5%. We should see important dynamical consequences of this, such as the systematic flattening of the slabs in this depth range for zones where deep-focus seismicity is present. There is no evidence for flattening in the case of the South American slab, nor an obvious pattern of flattening globally for slabs with deep focus events.
37. H. Kanamori, *Phys. Earth Planet. Inter.* **4**, 289 (1971); P. G. Silver and T. H. Jordan, *J. Geophys. Res.* **88**, 3273 (1983).
38. C. S. Lynnes and T. Lay, *ibid.* **93**, 13,407 (1988).
39. Other large-scale faults in the oceanic lithosphere, such as fracture zones, could also be sites of future deep focus events. Indeed, there is evidence that hydrothermal circulation penetrates into the mantle along these zones (S. Solomon, personal communication).
40. E. A. Okal *et al.*, *Geophys. Lett.*, in press.
41. T. Cahill and B. Isacks, *J. Geophys. Res.* **97**, 17,503 (1992).

42. We thank: the IRIS-PASSCAL program for supplying instruments and support, P. Soler, P. Baby, J. Telleria, and the San Calixto Observatory for providing logistical support, and M. Kikuchi and H. Kanamori for making their manuscripts available before publication. J. Dunlap assisted with manuscript preparation and M. Acierno with computer support. J. Vidale, S. Stein, and F. Press provided useful reviews. This work was supported by National Science Foundation grants EAR9304560, EAR9304949, EAR9304503, and the Carnegie Institution of Washington.

1 November 1994; accepted 26 January 1995